ACS Energy LETTERS

Cite This: ACS Energy Lett. 2018, 3, 2404−2409

http://pubs.acs.org/journal/aelccp

LETTER

High-Performance Alkaline Organic Redox Flow Batteries Based on 2-Hydroxy-3-carboxy-1,4-naphthoquinone

Caixing Wang,[†,⊥] Zhen Yang,[‡,⊥] Yanrong Wang,[†] Peiyang Zhao,[†] Wen Yan,[†] Guoyin Zhu,[†] Lianbo Ma,[†] Bo Yu,[†] Lei Wang,[†] Guigen Li,*[,‡,§] Jie Liu,[†,∥] and Zhong Jin*[,†]

[†]Key Laboratory of Mesoscopic Chemistry of MOE, School of Chemistry and Chemical Engineering, Nanjing University, Nanjing, Jiangsu 210093, China

[‡]Institute of Chemistry & BioMedical Sciences, Nanjing University, Nanjing, Jiangsu 210023, China

[§]Department of Chemistry and Biochemistry, Texas Tech University, Lubbock, Texas 79409-1061, United States

[∥]Department of Chemistry, Duke University, Durham, North Carolina 27708, United States

Supporting Information

ABSTRACT: **Aqueous redox flow batteries (ARFBs) based on the electrolyte solutions of redox-active organic molecules are very attractive for the application of large-scale electrochemical energy storage. We propose a high-performance ARFB system utilizing 2-hydroxy-3-carboxy-1,4-naphthoquinone (2,3-HCNQ) and $K_4Fe(CN)_6$ as the anolyte and catholyte active species, respectively. The 2,3-HCNQ molecule exhibits high solubility and can carry out a reversible two-electron redox process with rapid redox kinetics. The assembled 2,3-HCNQ/$K_4Fe(CN)_6$ ARFB delivered a cell voltage of 1.02 V and realized a peak power density of 0.255 W cm^{-2}. The 2,3-HCNQ/$K_4Fe(CN)_6$ ARFB can be stably operated at a current density of 100 mA cm^{-2} for long-term cycling (with a capacity retention of ∼94.7% after 100 cycles).**

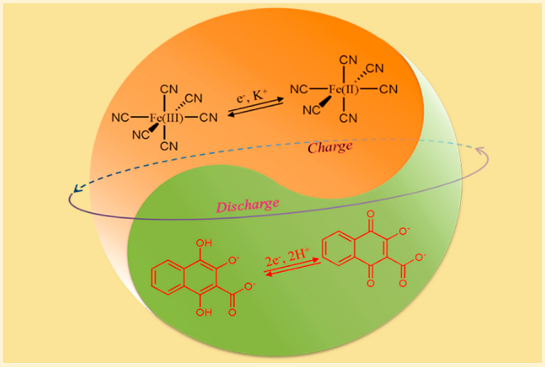

Redox flow batteries (RFBs) present a promising prospect in grid-scale energy storage, especially for mitigating the intermittent fluctuation of renewable energy sources, such as solar and wind power plants.[1−4] The operation of RFBs depends on the reversible electrochemical reactions of redox-active species dispersed in liquid-phase anolytes and/or catholytes.[5−8] The modular design of redox pairs should take into consideration several crucial properties, such as solubility, voltage window, reaction kinetics, cycling stability, etc. Over the past decade, great efforts have been made to develop aqueous redox flow batteries (ARFBs) that adopt water-soluble organic molecules in electrolytes.[9−14] Several classes of organic redox-active species, including quinone, viologen, alloxazine, 2,2,6,6-tetramethylpiperidinooxy (TEMPO), and their derivatives, have attracted considerable attention for the application in ARFBs, owing to the rapid redox kinetics, low corrosivity, high solubility, and low cost.[11−18] It is also known that organic molecules have excellent structural diversity; therefore, the electrochemical properties can be easily tailored by the modification of different functional groups.[19−29] Previous works suggested that the electron-donating groups can lower the redox potential, while the electron-withdrawing groups can elevate the redox potential, endowing the organic ARFBs with more flexible voltage regulation than traditional ARFBs.[12,14,19] Generally, the organic molecules often existed in negatively charged forms either in acidic or alkaline solutions during the whole charge−discharge process, so the crossover issue of active species through the separator can be overcome by employing a cation separator. It should be noticed that the redox species tending to release protons have higher solubility either in acid or alkaline solution, thus contributing to higher energy density and power density. For example, anthraquinone-sulfonic acid derived from anthraquinone can be dissolved with 1.0 M concentration in acid conditions.[13] In addition, the β-OH groups on the anthraquinone can significantly increase the solubility in the alkaline solution for improved proton dissociation in comparison with the α-OH groups.[14,27,29] Alloxazine-derived redox molecules also show improved solubility in the alkaline solution after the introduction of a carboxyl group or hydrotropic agent.[17,19] Given the fact that a

Received: July 22, 2018
Accepted: September 13, 2018
Published: September 13, 2018

DOI: 10.1021/acsenergylett.8b01296
ACS Energy Lett. 2018, 3, 2404−2409

large number of redox-active organic species have a relatively narrow voltage window and low solubility in water that may result in low volumetric energy density, it is vital to design novel organic molecular structures to fully satisfy the demands of ARFBs.

The derivatives of naphthoquinone often serve as electron acceptors in biochemical electron transport processes in organisms, such as photosynthesis[30−32] and aerobic respiration.[33,34] Ding et al. reported the use of naphthquinone derivates in organic RFBs.[35] Recently, naphthquinone functionalized with diethylene glycol monomethyl ether groups was reported to exhibit a high energy density (264 W h L^{-1}) in solvent-free organic redox flow batteries.[36] However, most quinone derivatives exhibit low solubility in water, which would limit the application in ARFBs. 2-Hydroxy-1,4-naphthoquinone (2-HNQ), also well-known as "lawsone", is a nature-abundant and low-cost red-orange dye that can be extracted from the leaves of henna trees and the flowers of water hyacinths. Each 2-HNQ molecule can undergo a reversible two-electron redox conversion between the quinone form and the phenol form, offering a potential of −0.70 V vs Ag/AgCl; thus, it can be used as a potential anolyte in ARFBs.[29] However, owing to the low solubility of 2-HNQ (0.48 M in alkaline solution) and the possible side reactions with O_2, the previous ARFB based on 2-HNQ anolyte (0.2 M) showed a low volumetric capacity and suffered from large capacity loss and poor cycling stability (<50% capacity retention per cycle at the low current density of 8 mA cm^{-2}). Therefore, 2-HNQ is inadequate to entirely fulfill the requirements for the application in ARFBs.

Here we report a mild and low-cost synthesis route to obtain a new negative redox-active naphthoquinone derivative organic material: 2-hydroxy-3-carboxy-1,4-naphthoquinone (2,3-HCNQ). The introduction of the hydroxyl and carboxyl groups decreases the redox potential of 2,3-HCNQ to −0.73 V vs Ag/AgCl and also greatly increases its solubility to 1.2 M in alkaline solution. The ARFB model based on alkaline 2,3-HCNQ anolyte matched with $K_4Fe(CN)_6$ catholyte in 1.0 M KOH (Figure 1) exhibits a cell voltage of 1.02 V, which is higher than those of acidic all-quinone or quinone-bromine ARFBs[11−13] and comparable to that of the alkaline ARFBs based on flavin mononucleotide (FMN) and 1,8-dihydroxyanthraquinone (1,8-DHAQ).[17,27] The 2,3-HCNQ molecule also exhibits other superior properties, including rapid redox kinetics, high ionization constants, and good electrochemical and thermal stability. Promoted by the rapid redox kinetics of 2,3-HCNQ, the 2,3-HCNQ/$K_4Fe(CN)_6$ ARFB can be stably operated at a current density of 100 mA cm^{-2} for long-term cycling (with a capacity retention of ∼94.7% after 100 cycles), which is comparable with that of existing alkaline and neutral ARFBs (Table S1).[14−27]

Through a facile and low-cost total synthesis route including a two-step cycloaddition step and an ester hydrolysis step, 2,3-HCNQ was synthesized with an overall yield of 70% (Figure 2a). Moreover, the synthesis cost of 2,3-HCNQ is very low, as estimated in Figure S1. Nuclear magnetic resonance (NMR) and liquid chromatography-tandem mass spectrometry (LC-MS) spectra confirm the formation of 2,3-HCNQ (Figures S2−S4). The cyclic voltammetry (CV) curves show that 2,3-HCNQ undergoes a reversible redox process in 1.0 M KOH on the glassy carbon electrode (GCE) (Figure 2b), corresponding to a formal potential (the average value of the anodic peak and cathodic peak potentials) of −0.73 V vs Ag/AgCl electrode (−0.52 V vs standard hydrogen electrode, SHE). As the sweep rates increases from 25 to 100 mV s^{-1}, the anodic−cathodic peak differences are still kept at ∼48 mV. Figure 2c shows the peak currents versus square roots of scan rates derivated from Figure 2b. According to the Randles−Sevcik equation (eq 1)

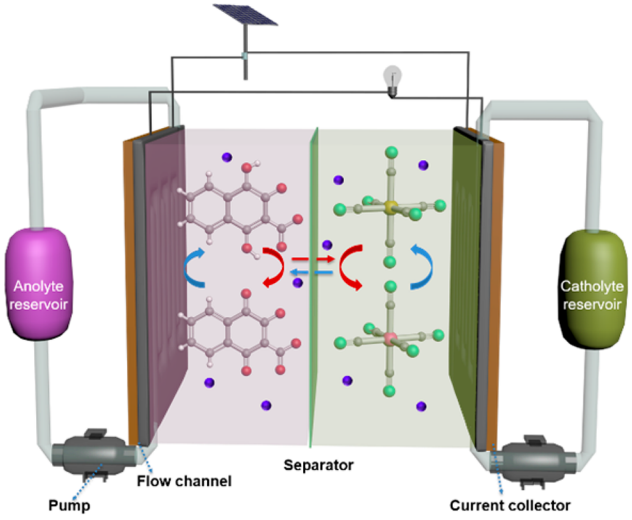

Figure 1. Cell configuration of ARFB based on 2,3-HCNQ anolyte and $K_4Fe(CN)_6$ catholyte. Both the anions are shown in ball-and-stick models (OH^- is omitted for clarity). During the charge process (blue arrows), 2,3-HCNQ is reduced to its phenol form, while ferrocyanide (pink balls for Fe(II)) is oxidized to ferricyanide (yellow balls for Fe(III)), and K^+ ions (blue balls) shift from catholyte to anolyte to balance the anion concentration. The discharge process is just the opposite (red arrows).

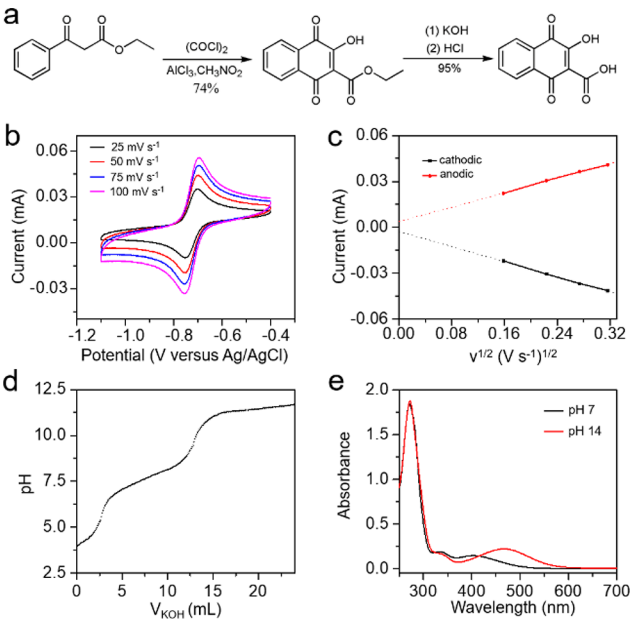

Figure 2. (a) Synthesis route of 2,3-HCNQ. (b) CV curves of 2 mM 2,3-HCNQ aqueous solution in 1.0 M KOH at different scan rates. (c) Peak currents vs square roots of scan rates. (d) Titration curve of 2,3-HCNQ (2.0 mL saturated 2,3-HCNQ solution (at pH 3.98) diluted to 40 mL and then titrated by 1.026 mM KOH standard solution). (e) UV−vis absorption spectra of 0.1 mM 2,3-HCNQ solution at pH 7 and pH 14.

DOI: 10.1021/acsenergylett.8b01296
ACS Energy Lett. 2018, 3, 2404−2409

$$i_p = 2.69 \times 10^5 \times An^{3/2}D^{1/2}Cv^{1/2} \quad (1)$$

the slope ratio of cathodic and anodic scans is calculated to be −1.04, which implies the 2,3-HCNQ and reduced 2,3-HCNQ molecules have similar diffusion coefficients.

To understand the influence of the additional carboxyl group, the ionization constants of 2,3-HCNQ were measured by the titration of standard KOH solution, and pK_{a1} and pK_{a2} were calculated to be 4.46 and 7.75 from the titration curve (Figure 2d), corresponding to the proton dissociation of carboxyl group and hydroxyl group on the backbone, respectively. The structural difference at different pH values was also determined via UV−vis absorption spectroscopy (Figure 2e). It shows that the absorption peaks of 2,3-HCNQ at pH 7 and pH 14 in ultraviolet band are similar, ascribed to the $\pi-\pi^*$ transition of the benzene ring. However, the absorption peaks in the visible band appear at 409 and 472 nm, respectively, owing to the presence of different ionization forms in neutral and alkaline solutions. Considering the adjacent effect, we propose that an intramolecular hydrogen bond is formed between the carboxylate anion and hydroxyl group at pH 7, while the negatively charged carboxylate anion and phenol anion repelled each other at pH 14 (Scheme S1a,b). To investigate the variation of deprotonation degree of 2,3-HCNQ at different oxidation states, the CV curves and the Pourbaix diagram at different pH values are measured (Figure S5). The CV curves show that 2,3-HCNQ undergoes a $2H^+-2e^-$ process over the whole pH range between 1.39−14. The Pourbaix diagram is almost a straight line when the pH is approaching to 14. This is different from previous reports of other quinones,[14,18] of which both oxidized and reduced forms are fully deprotonated. These results indicate that the reduced form of 2,3-HCNQ may not be fully deprotonated in the alkaline solution, probably owing to the formation of intramolecular hydrogen bonds and the restraint of already-dissociated dianion structure (Scheme S1c).

With the introduction of the carboxyl group, the formal potential of 2,3-HCNQ is negatively shifted by ∼30 mV compared to 2-HNQ (Figure S6a), which is abnormal for electron-withdrawing groups.[19] To understand this phenomenon, we also measured the UV−vis absorption spectrum of 2-HNQ in alkaline solution. Compared to 2-HNQ, the absorption peak of 2,3-HCNQ in visible band is positively shifted by ∼19 nm (Figure S6b). It indicates the conjugated effect between the carboxylate group and the backbone of naphthoquinone can effectively decrease the total molecule energy. Meanwhile, the carboxyl group tends to lose the proton in alkaline solution, thus contributing to the greatly improved solubility. According to the quantitative analysis of UV−vis absorption spectra (Figure S7), the solubility of 2,3-HCNQ in 1.0 M KOH is as high as 1.2 M at 20 °C, while the solubility of 2-HNQ in 1.0 M KOH is only ∼0.48 M, revealing the introduction of the carboxyl group can significantly enhance the solubility in alkaline solution, which confirms the importance of molecular structure design for ARFBs.

Notably, the stability of organic molecules has a great effect on the battery performance.[13,18] First, the electrochemical stability of 2,3-HCNQ was tested, as shown in Figure S8. The CV curve of 2,3-HCNQ solution at the 50th cycle is nearly overlapped with that at the first cycle. Moreover, the CV curve within a wide potential range from 0.2 to −1.4 V vs Ag/AgCl shows no additional peaks (Figure S8b), indicaing the absence of a side reaction and the good electrochemical stability.

Moreover, the thermal stability of 2,3-HCNQ is also investigated by thermogravimetric analysis (TGA), showing that 2,3-HCNQ can withstand elevated temperature up to 160 °C with no obvious mass loss (Figure S9). Subsequently, as the temperature progressively increased to 250 °C, the carboxyl group is removed and converted to CO_2, which accounts for ∼20% weight of 2,3-HCNQ (Mr: 217.95 g mol^{-1}, see Figure S4). When the temperature is higher than 250 °C, the naphthoquinone backbone will be gradually decomposed and carbonized. Thus, it is expected that 2,3-HCNQ can easily endure harsh temperatures. Considering the preparation conditions of ester hydrolysis step (heated in 10% KOH solution at 60 °C overnight), 2,3-HCNQ is proved to be chemically stable in alkaline solution, which is also conducive to the operation of ARFBs.

The diffusion coefficient (D) and rate constant (k_0) of 2,3-HCNQ were investigated by linear sweep voltammetry (LSV) method. Figure 3a shows the RDE curves at various rotation rates between 300 and 3000 rpm, and the well-defined plateau shapes indicate the mass-transport controlled limiting currents. Figure 3b illustrates the linear fitting of limiting currents against the square roots of rotation rates measured at −1.3 V vs Ag/AgCl. According to the Levich equation,[17] the diffusion coefficient of 2,3-HCNQ is calculated to be 3.44 × 10^{-6} cm^2 s^{-1} after background current calibration. Subsequently, a series of Koutecký−Levich plots obtained at different overpotentials between 5 and 300 mV are depicted (Figure 3c). The intercepts to the y axis represent the exchange currents (i_k) at specific overpotentials. The values of i_k were transformed to logarithm form to illustrate the Tafel plot (Figure 3d). Using the Butler−Volmer equation, the k_0 is calculated to be 2.07 × 10^{-3} cm s^{-1}, which is higher than that of common inorganic redox-active cations, such as VO^{2+}/VO^+, V^{3+}/V^{2+}, and Fe^{3+}/Fe^{2+}, implying that 2,3-HCNQ is a good candidate for anolyte material for alkaline ARFBs.[37]

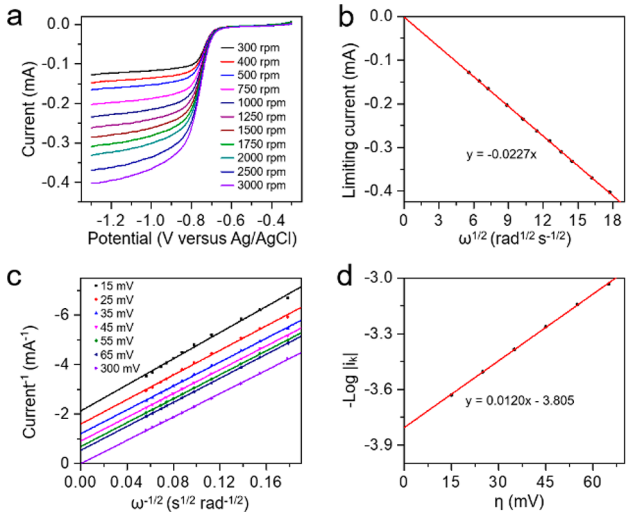

Figure 3. (a) RDE tests of 2 mM 2,3-HCNQ in 1.0 M KOH solution with a scan rate of 25 mV s^{-1} at different rotation rates between 300 and 3000 rpm. (b) Levich plot of the limiting currents vs the square roots of rotation rates. (c) Koutecký−Levich plots (the reciprocals of currents vs the square roots of rotation rates) derived from panel a at different overpotentials. (d) Fitting plot of Butler−Volmer equation derived from panel c at different overpotentials.

DOI: 10.1021/acsenergylett.8b01296
ACS Energy Lett. 2018, 3, 2404−2409

The electrochemical performances of 2,3-HCNQ/$K_4Fe(CN)_6$ ARFB were systematically tested. The anolyte is 5.0 mL of 0.5 M 2,3-HCNQ in 2.0 M KOH solution, and the catholyte is 15.0 mL of 0.4 M $K_4Fe(CN)_6$ in 1.0 M KOH solution. Nafion 212 membrane was used as the separator, and KOH-activated carbon paper with large active surface area was used as the electrode (Figure S10). The CV curves of 2 mM $K_4Fe(CN)_6$ and 2 mM 2,3-HCNQ solutions in 1.0 M KOH were measured separately, predicting a cell potential of 1.02 V (Figure 4a). To make sure the cell potential does not deviate from the charge−discharge plateaus owing to the possible rearrangement of organic redox-active species,[11,20,28] we used the galvanostatic intermittent titration technique (GITT) to more accurately evaluate the cell potential. Figure 4b shows the corresponding open-circuit voltages obtained at different states of charge (SOC). The open-circuit voltage at 10% SOC is 0.957 V. When the SOC is 50%, the open-circuit voltage is recorded to be 1.022 V, which is very close to the CV result.

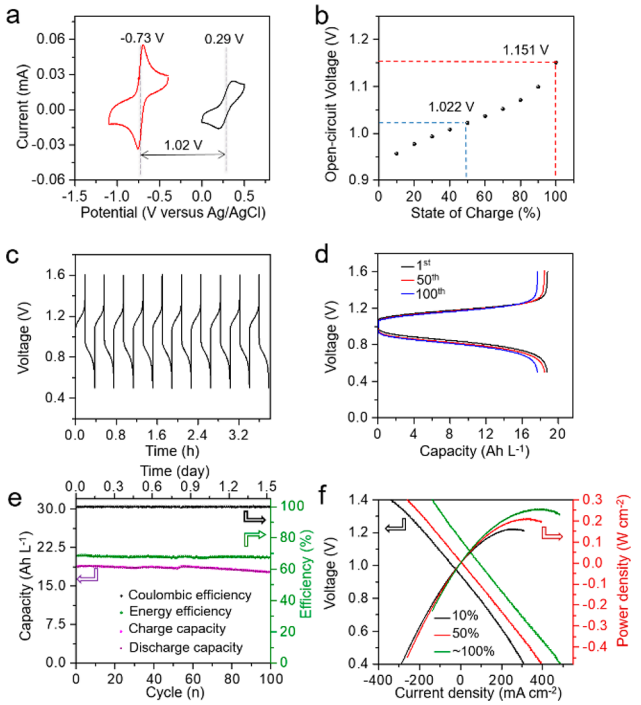

Figure 4. (a) CV curves of 2 mM 2,3-HCNQ (red trace) and 2 mM $K_4Fe(CN)_6$ (black trace) at 100 mV s^{-1} in 1.0 M KOH. (b) Open-circuit voltages of 2,3-HCNQ/$K_4Fe(CN)_6$ ARFB obtained at different states of charge by GITT method. (c) Voltage vs time curves of 2,3-HCNQ/$K_4Fe(CN)_6$ ARFB at 100 mA cm^{-2} recorded between the 1st and 10th cycles. (d) Galvanostatic charge−discharge curves of 2,3-HCNQ/$K_4Fe(CN)_6$ ARFB during the 1st, 50th, and 100th cycles at 100 mA cm^{-2}. (e) Cycling performance, Coulombic efficiencies, and energy efficiencies of 2,3-HCNQ/$K_4Fe(CN)_6$ ARFB at 100 mA cm^{-2}. (f) Polarization curves and areal power densities of the 2,3-HCNQ/$K_4Fe(CN)_6$ ARFB at 10%, 50%, and ∼100% SOC at 25 °C.

The voltage versus time curves of the initial 10 cycles at a current density of 100 mA cm^{-2} are shown in Figure 4c, indicating good cycling stability and reproducibility. The initial cycle time-anolyte volume ratio is calculated to be 272 s mL^{-1} $cycle^{-1}$, which is almost the same as that of 2,6-DHAQ/$K_4Fe(CN)_6$ ARFB,[14] indicating a similar anolyte utilization ratio. Concretely, the galvanostatic charge−discharge profiles (Figure 4d) show that the average charge and discharge voltages of the first cycle at 100 mA cm^{-2} are 1.19 and 0.84 V, respectively. The charge plateau is well-maintained for 100 cycles, while the discharge plateau is slightly decreased, likely because of the activity decay of carbon paper electrodes, not because of the increase of membrane impedance. The initial discharge capacity is 18.8 Ah L^{-1}, which is 70% of the theoretical capacity (26.8 Ah L^{-1}), and shows only a small attenuation after 100 cycles.

The cycling performance of 2,3-HCNQ/$K_4Fe(CN)_6$ ARFB is shown in Figure 4e. During the whole 100 cycles, the Coulombic efficiency is well-maintained at nearly 100%, and the energy efficiency is kept around 68.8%. The discharge capacity remains at 17.8 Ah L^{-1} after 100 cycles, corresponding to a retention ratio of 94.7%. The total charge−discharge time is ∼1.5 days, delivering a temporal capacity fade rate of 3.4% day^{-1} and an average Coulombic efficiency close to 100%. When the anolyte concentration was increased to 1.0 M (corresponding to 2.0 M electron concentration), the 2,3-HCNQ/$K_4Fe(CN)_6$ ARFB exhibited an initial discharge capacity of 41.0 Ah L^{-1} (Figure S11), which is ∼76.5% of the theoretical capacity limit at this concentration (53.6 Ah L^{-1}). The capacity of this cell decayed to 39.2 Ah L^{-1} after 20 cycles, showing a temporal capacity fade rate of 6.4% day^{-1}, possibly because of the anolyte decomposition and the small leakage of the cell.

As mentioned above, 2-HNQ suffers from severe capacity loss, possibly because of the interference of oxygen. For comparison, we measured the performance of 2-HNQ/$K_4Fe(CN)_6$ ARFB with 0.25 M concentration of 2-HNQ (Figure S12). Because of the lower solubility of 2-HNQ, higher concentration may result in the blockage of flow channels during the cycling processes. The 2-HNQ/$K_4Fe(CN)_6$ battery operated at 100 mA cm^{-2} shows a temporal fade rate of 4.1% day^{-1}, which is slightly higher than that of 2,3-HCNQ/$K_4Fe(CN)_6$ ARFB. These results indicate that the stability of these two naphthoquinone derivatives is comparable with that of 2,6-DHAQ but higher than that of 2,5-dihydroxy-1,4-benzoquinone in alkaline solution.[14,18]

Moreover, the symmetric flow cell based on 0.1 M 2,3-HCNQ solution was also tested by galvanostatic mode (Figure S13), showing a capacity retention of 94.1% after 50 cycles and a temporal capacity fade rate of 7.3% day^{-1}, comparable to the result of 2,6-DHAQ tested by potentiostatic mode.[38] The reasons for the different temporal capacity fade rates of full cell and symmetric cell might be due to the variations of decomposition rate, leakage rate, asymmetric polarized resistance, etc. Besides, we have performed a cycling pause at 0% SOC and 100% SOC of another symmetric cell based on 0.1 M 2,3-HCNQ solution with a resting time of 24 h to isolate the chemical stability of reduced and oxidized form of 2,3-HCNQ (Figure S14). The symmetric cell exhibits a fade rate of 0.6% day^{-1} and 13.4% day^{-1} at 0% SOC and 100% SOC at initial stage, respectively, indicating that the reduced form of 2,3-HCNQ is not very chemically stable, just like the other redox species.[38] Certainly, it should be admitted that the structure of naphthoquinones needs to be further optimized, similar to hydroxyanthraquinones.[39]

To evaluate the power output performance, the polarization curve of 2,3-HCNQ/$K_4Fe(CN)_6$ ARFB was recorded at different SOCs by LSV method (Figure 4f), because this method imposed minimal perturbation to the charge state compared to point-by-point galvanostatic holds.[14] The peak

DOI: 10.1021/acsenergylett.8b01296
ACS Energy Lett. 2018, 3, 2404−2409

power densities at 10%, 50%, and ∼100% SOCs are calculated to be 0.162, 0.211, and 0.255 W cm^{-2}, respectively. The peak power denisties measured here are higher than FMN/$K_4Fe(CN)_6$ and 1,8-DHAQ/$K_4Fe(CN)_6$ ARFBs at room temperature,[17,27] which is ascribed to higher concentration of 2,3-HCNQ anolyte.

In summary, we propose that the rationally designed 2,3-HCNQ molecule with good electrochemical properties and high solubility is a promising candidate for anolyte material for alkaline ARFBs. Benefitting from the rapid kinetic rates of both catholyte and anolyte, the 2,3-HCNQ/$K_4Fe(CN)_6$ ARFB can be stably operated at a current density of 100 mA cm^{-2} for more than 100 cycles without any noble metal electrocatalyst. Moreover, 2,3-HCNQ is composed of earth-abundant elements and can be synthesized at very low cost, which is beneficial for the sustainable use of the society. It is also promising to combine the 2,3-HCNQ/$K_4Fe(CN)_6$ ARFB with other inexpensive, stable, and highly ion-selective membranes[39,40] to further lower its capital cost for large-scale energy storage applications.

■ ASSOCIATED CONTENT

Supporting Information

The Supporting Information is available free of charge on the ACS Publications website at DOI: 10.1021/acsenergylett.8b01296.

Experimental section and additional figures and tables (PDF)

■ AUTHOR INFORMATION

Corresponding Authors

*E-mail: zhongjin@nju.edu.cn.
*E-mail: guigenli@nju.edu.cn.

ORCID

Jie Liu: 0000-0003-0451-6111
Zhong Jin: 0000-0001-8860-8579

Author Contributions

⊥C.W. and Z.Y. contributed equally.

Notes

The authors declare no competing financial interest.

■ ACKNOWLEDGMENTS

This work is supported by National Key R&D Program of China (2017YFA0208200, 2016YFB0700600, and 2015CB659300), Projects of NSFC (21872069, 51761135104, 21573108, and 21332005), High-Level Entrepreneurial and Innovative Talents Program of Jiangsu Province, and the Fundamental Research Funds for the Central Universities (020514380146).

■ REFERENCES

(1) Dunn, B.; Kamath, H.; Tarascon, J. M. Electrical Energy Storage for the Grid: A Battery of Choices. *Science* **2011**, *334*, 928−935.
(2) Wang, W.; Luo, Q.; Li, B.; Wei, X.; Li, L.; Yang, Z. Recent Progress in Redox Flow Battery Research and Development. *Adv. Funct. Mater.* **2013**, *23*, 970−986.
(3) Yang, Z. G.; Zhang, J. L.; Kintner-Meyer, M. C. W.; Lu, X. C.; Choi, D. W.; Lemmon, J. P.; Liu, J. Electrochemical Energy Storage for Green Grid. *Chem. Rev.* **2011**, *111*, 3577−3613.
(4) Zhao, Y.; Ding, Y.; Li, Y.; Peng, L.; Byon, H. R.; Goodenough, J. B.; Yu, G. A Chemistry and Material Perspective on Lithium Redox Flow Batteries towards High-Density Electrical Energy Storage. *Chem. Soc. Rev.* **2015**, *44*, 7968−7996.
(5) Kjeang, E.; Michel, R.; Harrington, D. A.; Djilali, N.; Sinton, D. A Microfluidic Fuel Cell with Flow-through Porous Electrodes. *J. Am. Chem. Soc.* **2008**, *130*, 4000−4006.
(6) Chen, X.; Hopkins, B. J.; Helal, A.; Fan, F. Y.; Smith, K. C.; Li, Z.; Slocum, A. H.; McKinley, G. H.; Carter, W. C.; Chiang, Y.-M. A Low-Dissipation, Pumpless, Gravity-Induced Flow Battery. *Energy Environ. Sci.* **2016**, *9*, 1760−1770.
(7) Marschewski, J.; Brenner, L.; Ebejer, N.; Ruch, P.; Michel, B.; Poulikakos, D. 3D-Printed Fluidic Networks for High-Power-Density Heat-Managing Miniaturized Redox Flow Batteries. *Energy Environ. Sci.* **2017**, *10*, 780−787.
(8) Noack, J.; Roznyatovskaya, N.; Herr, T.; Fischer, P. The Chemistry of Redox-Flow Batteries. *Angew. Chem., Int. Ed.* **2015**, *54*, 9776−9809.
(9) Winsberg, J.; Hagemann, T.; Janoschka, T.; Hager, M. D.; Schubert, U. S. Redox-Flow Batteries: From Metals to Organic Redox-Active Materials. *Angew. Chem., Int. Ed.* **2017**, *56*, 686−711.
(10) Xu, Y.; Wen, Y. H.; Cheng, J.; Cao, G. P.; Yang, Y. S. A Study of Tiron in Aqueous Solutions for Redox Flow Battery Application. *Electrochim. Acta* **2010**, *55*, 715−720.
(11) Yang, B.; Hoober-Burkhardt, L.; Wang, F.; Surya Prakash, G. K.; Narayanan, S. R. An Inexpensive Aqueous Flow Battery for Large-Scale Electrical Energy Storage Based on Water-Soluble Organic Redox Couples. *J. Electrochem. Soc.* **2014**, *161*, A1371−A1380.
(12) Huskinson, B.; Marshak, M. P.; Suh, C.; Er, S.; Gerhardt, M. R.; Galvin, C. J.; Chen, X.; Aspuru-Guzik, A.; Gordon, R. G.; Aziz, M. J. A Metal-Free Organic-Inorganic Aqueous Flow Battery. *Nature* **2014**, *505*, 195−198.
(13) Gerhardt, M. R.; Tong, L.; Gómez-Bombarelli, R.; Chen, Q.; Marshak, M. P.; Galvin, C. J.; Aspuru-Guzik, A.; Gordon, R. G.; Aziz, M. J. Anthraquinone Derivatives in Aqueous Flow Batteries. *Adv. Energy Mater.* **2017**, *7*, 1601488.
(14) Lin, K. X.; Chen, Q.; Gerhardt, M. R.; Tong, L. C.; Kim, S. B.; Eisenach, L.; Valle, A. W.; Hardee, D.; Gordon, R. G.; Aziz, M. J.; et al. Alkaline quinone flow battery. *Science* **2015**, *349*, 1529−1532.
(15) Janoschka, T.; Martin, N.; Martin, U.; Friebe, C.; Morgenstern, S.; Hiller, H.; Hager, M. D.; Schubert, U. S. An Aqueous, Polymer-Based Redox-Flow Battery Using Non-Corrosive, Safe, and Low-Cost Materials. *Nature* **2015**, *527*, 78−81.
(16) Liu, T.; Wei, X.; Nie, Z.; Sprenkle, V.; Wang, W. A Total Organic Aqueous Redox Flow Battery Employing a Low Cost and Sustainable Methyl Viologen Anolyte and 4-HO-TEMPO Catholyte. *Adv. Energy Mater.* **2016**, *6*, 1501449.
(17) Orita, A.; Verde, M. G.; Sakai, M.; Meng, Y. S. A Biomimetic Redox Flow Battery Based on FLavin Mononucleotide. *Nat. Commun.* **2016**, *7*, 13230.
(18) Yang, Z. J.; Tong, L. C.; Tabor, D. P.; Beh, E. S.; Goulet, M. A.; De Porcellinis, D.; Aspuru-Guzik, A.; Gordon, R. G.; Aziz, M. J. Alkaline Benzoquinone Aqueous Flow Battery for Large-Scale Storage of Electrical Energy. *Adv. Energy Mater.* **2018**, *8*, 1702056.
(19) Lin, K. X.; Gomez-Bombarelli, R.; Beh, E. S.; Tong, L. C.; Chen, Q.; Valle, A.; Aspuru-Guzik, A.; Aziz, M. J.; Gordon, R. G. A Redox-Flow Battery with an Alloxazine-Based Organic Electrolyte. *Nature Energy* **2016**, *1*, 16102.
(20) Janoschka, T.; Martin, N.; Hager, M. D.; Schubert, U. S. An Aqueous Redox-Flow Battery with High Capacity and Power: The TEMPTMA/MV System. *Angew. Chem., Int. Ed.* **2016**, *55*, 14427−14430.
(21) Hu, B.; DeBruler, C.; Rhodes, Z.; Liu, T. L. Long-Cycling Aqueous Organic Redox Flow Battery (AORFB) towards Sustainable and Safe Energy Storage. *J. Am. Chem. Soc.* **2017**, *139*, 1207−1214.
(22) Beh, E. S.; De Porcellinis, D.; Gracia, R. L.; Xia, K. T.; Gordon, R. G.; Aziz, M. J. A Neutral pH Aqueous Organic-Organometallic Redox Flow Battery with Extremely High Capacity Retention. *ACS Energy Lett.* **2017**, *2*, 639−644.
(23) Winsberg, J.; Janoschka, T.; Morgenstern, S.; Hagemann, T.; Muench, S.; Hauffman, G.; Gohy, J. F.; Hager, M. D.; Schubert, U. S.

DOI: 10.1021/acsenergylett.8b01296
ACS Energy Lett. 2018, 3, 2404−2409

Poly(TEMPO)/Zinc Hybrid-Flow Battery: A Novel, "Green," High Voltage, and Safe Energy Storage System. *Adv. Mater.* **2016**, *28*, 2238−2243.
(24) Winsberg, J.; Stolze, C.; Schwenke, A.; Muench, S.; Hager, M. D.; Schubert, U. S. Aqueous 2,2,6,6-Tetramethylpiperidine-N-oxyl Catholytes for a High-Capacity and High Current Density Oxygen-Insensitive Hybrid-Flow Battery. *ACS Energy Lett.* **2017**, *2*, 411−416.
(25) Leung, P. K.; Martin, T.; Shah, A. A.; Anderson, M. A.; Palma, J. Membrane-Less Organic-Inorganic Aqueous Flow Batteries with Improved Cell Potential. *Chem. Commun.* **2016**, *52*, 14270−14273.
(26) Luo, J.; Hu, B.; Debruler, C.; Liu, T. L. A "π-Conjugation Extended Viologen" as Novel Two-Electron Storage Anolyte for Total Organic Aqueous Redox Flow Battery. *Angew. Chem., Int. Ed.* **2018**, *57*, 231.
(27) Cao, J.; Tao, M.; Chen, H.; Xu, J.; Chen, Z. A Highly Reversible Anthraquinone-Based Anolyte for Alkaline Aqueous Redox Flow Batteries. *J. Power Sources* **2018**, *386*, 40−46.
(28) Hoober-Burkhardt, L.; Krishnamoorthy, S.; Yang, B.; Murali, A.; Nirmalchandar, A.; Prakash, G. K. S.; Narayanan, S. R. A New Michael-Reaction-Resistant Benzoquinone for Aqueous Organic Redox Flow Batteries. *J. Electrochem. Soc.* **2017**, *164*, A600−A607.
(29) Wedege, K.; Drazevic, E.; Konya, D.; Bentien, A. Organic Redox Species in Aqueous Flow Batteries: Redox Potentials, Chemical Stability and Solubility. *Sci. Rep.* **2016**, *6*, 39101.
(30) Sebban, P.; Maroti, P.; Hanson, D. K. Electron and Proton-Transfer to the Quinones in Bacterial Photosynthetic Reaction Centers - Insight from Combined Approaches of Molecular-Genetics and Biophysics. *Biochimie* **1995**, *77*, 677−694.
(31) Weyers, A. M.; Chatterjee, R.; Milikisiyants, S.; Lakshmi, K. V. Structure and Function of Quinones in Biological Solar Energy Transduction: A Differential Pulse Voltammetry, EPR, and Hyperfine Sublevel Correlation (HYSCORE) Spectroscopy Study of Model Benzoquinones. *J. Phys. Chem. B* **2009**, *113*, 15409−15418.
(32) Hanson, D. K.; Baciou, L.; Tiede, D. M.; Nance, S. L.; Schiffer, M.; Sebban, P. Bacterial Reaction Centers Protons Can Diffuse to the Secondary Quinone by Alternative Pathways. *Biochim. Biophys. Acta, Bioenerg.* **1992**, *1102*, 260−265.
(33) Horsefield, R.; Yankovskaya, V.; Sexton, G.; Whittingham, W.; Shiomi, K.; Omura, S.; Byrne, B.; Cecchini, G.; Iwata, S. Structural and Computational Analysis of the Quinone-Binding Site of Complex II (succinate-ubiquinone oxidoreductase) - A Mechanism of Electron Transfer and Proton Conduction during Ubiquinone Reduction. *J. Biol. Chem.* **2006**, *281*, 7309−7316.
(34) Sun, F.; Huo, X.; Zhai, Y.; Wang, A.; Xu, J.; Su, D.; Bartlam, M.; Rao, Z. Crystal Structure of Mitochondrial Respiratory Membrane Protein Complex II. *Cell* **2005**, *121*, 1043−1057.
(35) Ding, Y.; Li, Y. F.; Yu, G. H. Exploring Bio-inspired Quinone-Based Organic Redox Flow Batteries: A Combined Experimental and Computational Study. *Chem.* **2016**, *1*, 790−801.
(36) Shimizu, A.; Takenaka, K.; Handa, N.; Nokami, T.; Itoh, T.; Yoshida, J. Liquid Quinones for Solvent-Free Redox Flow Batteries. *Adv. Mater.* **2017**, *29*, 1606592.
(37) Liao, S.; Zong, X.; Seger, B.; Pedersen, T.; Yao, T.; Ding, C.; Shi, J.; Chen, J.; Li, C. Integrating a Dual-Silicon Photoelectrochemical Cell into a Redox Flow Battery for Unassisted Photocharging. *Nat. Commun.* **2016**, *7*, 11474.
(38) Goulet, M. A.; Aziz, M. J. Flow Battery Molecular Reactant Stability Determined by Symmetric Cell Cycling Methods. *J. Electrochem. Soc.* **2018**, *165*, A1466−A1477.
(39) Kwabi, D. G.; Lin, K. X.; Ji, Y. L.; Kerr, E. F.; Goulet, M. A.; De Porcellinis, D.; Tabor, D. P.; Pollack, D. A.; Aspuru-Guzik, A.; Gordon, R. G.; et al. Alkaline Quinone Flow Battery with Long Lifetime at pH 12. *Joule* **2018**, DOI: 10.1016/j.joule.2018.07.005.
(40) De Porcellinis, D.; Mecheri, B.; D'Epifanio, A.; Licoccia, S.; Granados-Focil, S.; Aziz, M. J. Communication—Sulfonated Poly (ether ether ketone) as Cation Exchange Membrane for Alkaline Redox Flow Batteries. *J. Electrochem. Soc.* **2018**, *165*, A1137−A1139.

DOI: 10.1021/acsenergylett.8b01296
ACS Energy Lett. 2018, 3, 2404−2409